J Solid State Electrochem (2013) 17:191–199
DOI 10.1007/s10008-012-1883-4

ORIGINAL PAPER

Tetragonal to monoclinic phase transition observed during Zr anodisation

Francisco Trivinho-Strixino · Donizete X. da Silva · Carlos O. Paiva-Santos · Ernesto C. Pereira

Received: 25 September 2011 / Revised: 11 September 2012 / Accepted: 14 September 2012 / Published online: 22 September 2012

Abstract Plasma electrolytic oxidation (PEO) is a coating procedure that utilises anodic oxidation in aqueous electrolytes above the dielectric breakdown voltage to produce oxide coatings that have specific properties. These conditions facilitate oxide formation under localised high temperatures and pressures that originate from short-lived microdischarges at sites over the metal surface and have fast oxide volume expansion. Anodic ZrO_2 films were prepared by subjecting metallic zirconium to PEO in acid solutions ($H_2C_2O_4$ and H_3PO_4) using a galvanostatic DC regime. The ZrO_2 microstructure was investigated in films that were prepared at different charge densities. During the anodic breakdown, an important change in the amplitude of the voltage oscillations at a specific charge density was observed (i.e., the transition charge density (Q^T)). We verified that this transition charge is a monotonic function of both the current density and temperature applied during the anodisation, which indicated that Q^T is an intrinsic response of this system. The oxide morphology and microstructure were characterised using SEM and X-ray diffraction experiments (XRD) techniques. X-ray diffraction analysis revealed that the change in voltage oscillation was correlated with oxide microstructure changes during the breakdown process.

Keywords Valve metals · ZrO_2 · Anodic films · Anodic breakdown · Microstructure · Phase transformation · Plasma electrolytic oxidation (PEO)

F. Trivinho-Strixino
Departamento de Física, Química e Matemática,
Universidade Federal de São Carlos,
São Carlos, SP, Brazil

C. O. Paiva-Santos
Laboratório Computacional de Análises Cristalográficas e Cristalinas, Depto de Físico-Química, Instituto de Química,
Universidade Estadual Paulista,
Araraquara, SP, Brazil

E. C. Pereira (✉)
Departamento de Química, Universidade Federal de São Carlos,
Rod. Washington Luis Km 235, Cx 676,
São Carlos, SP, Brazil
e-mail: decp@power.ufscar.br

Present Address:
D. X. da Silva
Universidade Federal de Tocantins,
Palmas, TO, Brazil

Introduction

Anodic oxide films on valve metals have been investigated since the 1950s [1–5]. The electronic, electrochemical and optical properties of these materials motivated our study in this area due to the different technological applications and the interesting fundamental aspects of oxide growth for protective coatings. Recently, interest in these materials has increased due to the potential for morphological and composition control on anodic alumina [6–8] and other valve metal oxides [9–14] produced by plasma electrolytic oxidation (PEO).

During the oxide growth at the galvanostatic DC regime, the film thickness increases until it reaches a critical value. At this stage, an oxide rupture can occur, which is known as an electrolytic breakdown. This process is characterised by a decrease in the oxide growth rate, potential oscillations caused by the destruction and healing processes in the oxide film, and visible sparks over the surface of the substrate [3, 15–17]. Experimental observations reveal that the electrolytic breakdown phenomenon depends on various experimental parameters, such as electrolyte composition [18–20], applied current density [21–24] and solution temperature

[25]. A number of theoretical models have been proposed to explain the electrolytic breakdown, such as electron avalanche [26–28], mechanical breakdown [29, 30] and pit formation [31, 32]. However, due to the complexity of this process, a complete mechanistic overview regarding the breakdown of valve metal oxides under high field regime is under discussion [4, 15, 33, 34].

Although many studies have been published on the mechanism and characteristics of the breakdown potential [3, 26–28, 35, 36], only a few address the potential oscillation behaviour inside this region in detail, and its relationship with the oxide microstructure is rarely seen [37–39]. Previous reports have described these oxides as being amorphous or crystalline [40] depending on the nature of the metal and the experimental conditions used for their preparation. The oxides formed on aluminium, niobium and tantalum are normally amorphous, and those prepared on zirconium [1, 3, 37, 41, 42] and hafnium are often crystalline [3, 40, 43]. Both types of microstructures were found in electrochemically prepared TiO_2 [3, 44]. The generally proposed crystallisation mechanism that has been described in the literature states that it could occur by nucleation or by conversion of an amorphous phase into a crystalline phase [1, 41]. In this case, the mechanical stresses in the outer oxide layers could lead to the formation of cracks during electrolytic breakdown, which could facilitate the electrolyte penetration into these cracks. Consequently, the electrolyte transport to the metal–oxide interface could be responsible for initiating the conversion of the crystalline phase [1, 41]. Another possibility is that crystallisation could occur in the outer-layer region of the oxide phase [2, 45, 46]. In this case, the crystallisation process could be related to complex phenomena, such as the electrolyte composition, a temperature increase in the film due to the presence of sparks, the high electric field generated or the localised high current density observed during the PEO process [15, 46]. However, a complete explanation regarding the microstructure changes inside the breakdown region on the valve metals is still missing.

The microstructure data of ZrO_2 films have been addressed in many papers [3, 37, 44, 47–57]. However, these papers only described the properties of thin, passivated films (in the order of a few nanometres). There are also several studies that have investigated the microstructure of thermally prepared ZrO_2 [52–57]. A recently published study described the microstructure changes and the internal stress effects observed in ZrO_2 that was obtained by PEO. The authors focused their description only in the earlier stages of the oxide breakdown, which has an applied charge density of 0.5 °C cm^{-2} [37]; however, they missed the long regime PEO where thicker oxides can be obtained. We believe that the study of anodic oxides that are produced after a long breakdown regime is of great importance to understand the rupture phenomena and to improve the synthetic knowledge of novel and protective coating materials for different technological applications. From this perspective, we present results regarding the morphology and microstructure changes of ZrO_2 during galvanostatic DC PEO after the breakdown region.

Materials and methods

Reagents and anodisation experiments

ZrO_2 films were prepared at a constant current density over Zr metallic electrodes (Aldrich® and Alfa Aesar®, 99.8 %, 0.25 mm thick, annealed). The electrodes were previously polished using fine-grain sandpaper with grades up to 600 and 1,200. Two Pt sheets were used as counter electrodes to obtain a homogeneous electric field distribution over the electrode surfaces during anodisation. Film growth was carried out in acid solution (oxalic acid or phosphoric acid, PA, Merck®) at various concentrations, current densities and temperatures. We selected specific experimental conditions for anodisation that exhibited the transition charge density (Q^T) and were reproducible. A homemade power source was used to anodise the Zr electrode, and data acquisition was performed using an HP 34410A Digital Multimeter that was connected to a computer to register the voltage/time curves. The acquisition software was built using the HP-VEE 5.0® interface software.

Microstructural and morphological analyses

Microstructure characterisation of the ZrO_2 films was performed using an X-ray diffractometer (Siemens model D-5000) with $Cu_{K\alpha}$ radiation (lambda=1.5406 Å). The X-ray diffraction data were collected with 2theta steps of 0.02° in a range from 20° to 120°. The Le Bail method [58] was applied, and the isotropic strain and the crystallite sizes were evaluated. For this purpose, the GSAS Suite [59] was used with the EXPGUI interface [60]. To improve the X-ray diffraction experiments (XRD) analyses, we selected only one experimental condition (applied current density, electrolyte composition and temperature) and prepared seven distinct samples with different charge densities before and after the charge transition density (Q^T). The morphological characterisation was carried out using a SEM Zeiss® DSM 940A.

Results

Figure 1 illustrates typical curves for the Zr anodisation in 0.05 mol L^{-1} oxalic acid or 0.1 mol L^{-1} PA. Initially, the voltage increase indicates that the ZrO_2 film thickness increased [3, 5, 37]. Assuming that the voltage is a linear

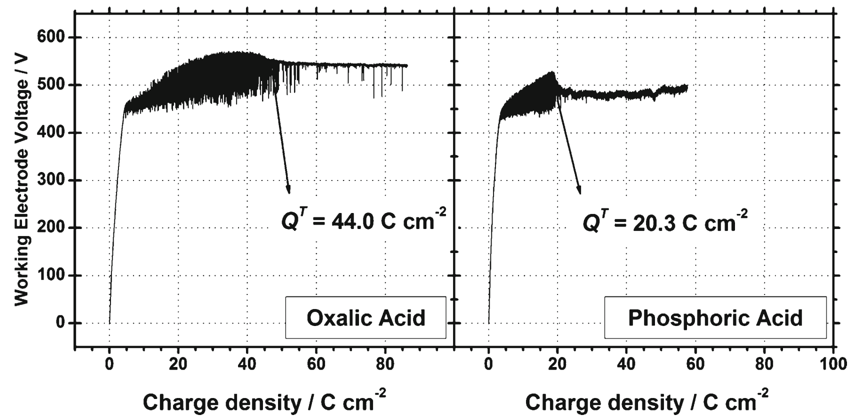

Fig. 1 Voltage–charge curve for Zr anodisation in 0.05 mol L^{-1} oxalic acid solution, i= 24 mA cm^{-2}, T=25 °C and 0.1 mol L^{-1} phosphoric acid solution, i=16 mA cm^{-2}, T= 20 °C

function of the charge and considering that the oxide molar volume is constant, under the galvanostatic DC PEO regime, this region could be associated with film growth that is controlled mainly by the ionic current [3, 5]. Of course, this is an ideal situation, and some small deviations from linearity may appear. These deviations could be related to side effects that occur during oxide growth, such as surface effects (flaws), non-constant oxide volume growth, spatial charge distribution and the possibility of non-coherent oxide film formation [5, 37, 61]. As can be observed in Fig. 1, the onset of electrolytic breakdown occurs at higher charge values. After this stage, a large decrease in the anodisation rate (dE/dQ) is observed, and sharp voltage oscillations appear. This behaviour indicates a rupture in the oxide, which could be related to electronic [26] or mechanical processes [29]. For zirconium anodisation, the initial voltage oscillation amplitude increase can be explained in terms of localised breakdown events that occur at surface defects over the film [5, 35, 62]. The presence of these defects originates either from the metal/oxide interface or from the oxide/electrolyte interface [35], and these lead to irregularities in the oxide microstructure. After each breakdown event, the current is concentrated in these defects, causing local repassivation at these points [62]. In addition, fast simultaneous destruction and healing processes in these areas can explain the sharp voltage oscillations that are observed between 4.3 and 40.0 °C cm^{-2} for anodisation in the oxalic acid solution or between 3.2 and 20.0 °C cm^{-2} for anodisation in the PA solution (Fig. 1). Visual sparks were also detected in this region. According to some authors, the presence of sparks in the substrate surface and their intensity, size and lifetime could be associated with the potential oscillations observed in this region [15–17, 63–65]. As the anodisation continues, the voltage oscillation amplitude decreases quickly at charge densities higher than 44.0 °C cm^{-2} or 20.3 °C cm^{-2} (here named transition charge density, Q^T) for the oxalic and PA solutions, respectively.

To study this transition (Q^T) in more detail, we performed several measurements using different experimental conditions, changing the current density, electrolyte concentration and temperature, as shown in Fig. 2. Variation in the electrolyte concentration had no effect on Q^T; therefore, this parameter was removed from the analysis. On the other hand, the current density and the electrolyte temperature were monotonic functions of Q^T (Fig. 2). In this figure, one can see that Q^T increases with applied current density, whereas it falls as electrolyte temperature rises. This observation indicates that this transition (Q^T) is an intrinsic behaviour of this system and not an experimental artefact. The dependence of Q^T on both the current density and the temperature suggests that this parameter should be controlled by kinetics. Variation of the applied current density will change the electrical field across the film, and consequently, all corresponding processes would be influenced by this parameter. For instance, an increase in the current density may change the cationic and anionic current components ratio, i.e., the transport number, due to the increase of the cationic transport observed for Zr anodisation [3, 18, 66]. Hence, the specific molar volume ratio between the metal and the oxide, which is known as the Pilling–Bedworth coefficient, would be affected. This last parameter relates to the transport of charged species, which can alter the microstructure and mechanical strain that originated during anodisation [67–69]. The variation of the electric field could also modify the kinetics of the electrochemical reactions that occur in the oxide/electrolyte interface due to the selective control of ionic species that are being absorbed in specific localised sites at the oxide surface. This effect could lead to an increase in the oxide dissolution rate that is caused by the presence of soluble electrolyte salts that are deposited over the oxide [70].

On the other hand, multiple factors need to be taken account of with respect to the electrolyte temperature. According to theoretical models that are described in the literature [26, 35], the rupture potential is a logarithmic function with respect to the electrolyte resistivity [26]. Hence, the electrolyte resistivity will affect the oxide dissolution kinetics and the discharge reactions over the surface during anodisation. As a result, there is a local rise in the temperature of the film that is caused by plasma generation

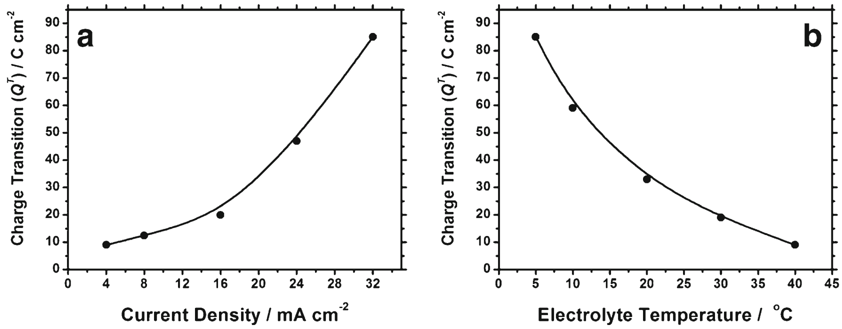

Fig. 2 Transition charge density (Q^T) as a function of applied current density (**a**) and electrolyte temperature (**b**). Oxide films were prepared in 0.05 molL^{-1} oxalic acid solution

from the PEO process. All of these side effects (i.e., rupture potential, electrolyte resistivity, dissolution kinetics, discharge reactions, local rise of temperature and plasma generation) led us to conclude that this system is filled with highly complicated transient interconnected processes. The oscillatory mechanism during anodic oxide growth has already been studied [26, 35, 71–75]; however, no charge transition after long breakdown regime has been described. It is well established in the literature that the breakdown phenomenon is mainly dependent on the properties of the oxide/solution interface [5, 22, 25, 29], which depend on the local electric field and the solution temperature. Owing to the high complexity of these transient systems under the breakdown regime, a complete mechanistic interpretation of the parameter Q^T and its dependence with the preparation parameters (applied current density, electrolyte composition temperature and composition) is difficult to establish and is beyond the scope of this study. Potential explanations for the potential oscillation variation include the localised destruction/healing phenomena and the decreasing intensity of the visual spark events over the oxide surface which changes the local temperature reaction. Therefore, a change in the amplitude of this parameter could be related to how deep the destruction process occurs in the outer oxide layer and to how the kinetics of the remaining healing process over these destructed areas modify the new oxide nature. If this relationship is true, a change in the physical properties of the oxide must occur, i.e., the macroscopic and microscopic properties of the oxide might be different before and after Q^T. Therefore, to investigate this proposition, morphological and microstructural characterisations of the ZrO_2 films were performed.

The morphological analyses are illustrated in Fig. 3. The basic morphology is characterised by the presence of blisters and holes that are distributed over the whole surface of ZrO_2 after 12.8 °C cm^{-2}. Similar results were obtained by the anodic oxidation of zirconium when previously covered with a thin aluminium layer. Shimizu et al. [76] studied the ion transport process inside the oxide during its formation. The mechanism of blister formation was proposed to be a combination of stress generation during oxidation of the inner zirconium layer and the relatively poor adhesion

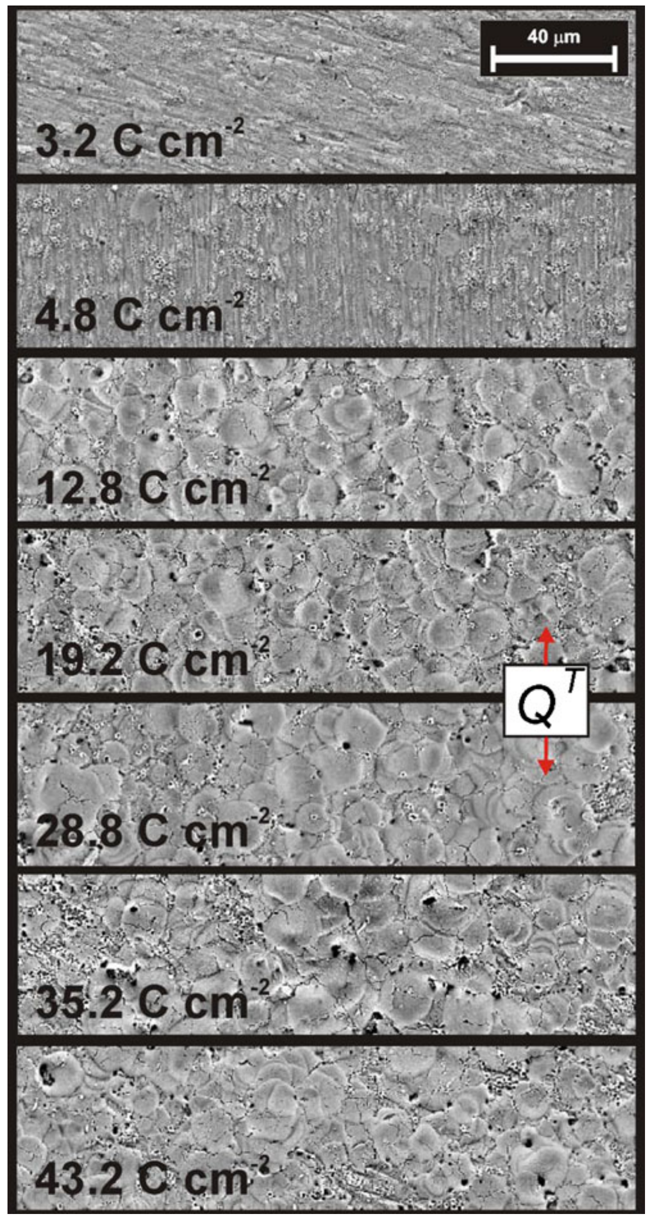

Fig. 3 Scanning electron microscope top-view photographs of ZrO_2 films anodised in 0.1 molL^{-1} phosphoric acid solution, i=16 mAcm^{-2}, T=20 °C, prepared with different charge densities. Q^T is situated between oxide samples anodised with 19.2 Ccm^{-2} and 28.8 °Ccm^{-2}

between the Al_2O_3 and ZrO_2. In the present case (Zr anodisation only), we believe that the origin of the blisters could be associated with the presence of oxygen gas bubbles generated on the electrode surface during the metal PEO. The lifetime of the bubbles adsorbed on the electrode surface could be long enough to inhibit solution access in that region, causing the "blister structure". Nevertheless, there is no difference in the morphology before and after Q^T, indicating that the morphology could not be directly associated to the potential oscillation transition (Fig. 3).

The microstructural analyses, which were performed using XRD, are illustrated in Fig. 4. First, it is important to stress that the oxide microstructure is the same for both oxides prepared in different electrolytes (oxalic acid or PA), i.e., the major phase that is present in the oxide is the monoclinic phase. However, herein, we present the analysis of the XRD patterns for oxide film prepared in only one electrolyte: 0.1 $mol L^{-1}$ PA.

At atmospheric pressure, the existence of the three polymorphs of ZrO_2 has been described in the literature, i.e., monoclinic, tetragonal and cubic [54]. The low-temperature monoclinic phase transforms into the tetragonal phase at 1,170 °C and into the cubic phase at 2,370 °C. Using thermal preparation procedures, the cubic and tetragonal phases can be stabilised at room temperature by the addition of dopants, such as Mg, Ca or Y [54]. The same type of result has been observed for anodically prepared ZrO_2 in the presence of Ca or Mg ions in the electrolyte solution [12]. In the absence of dopants, the monoclinic phase is predominant. In Fig. 4, the main XRD peaks for the monoclinic phase are observed at 2theta=28.15° and 31.48°; however, there was only one main peak observed at 2theta=30.20° for the tetragonal phase. The cubic phase was not detected in our samples. Therefore, from Fig. 4, one can conclude that the monoclinic and tetragonal phases are present in distinct quantities for different anodisation charges. For those spectra in which the reflections of the metallic Zr (hexagonal phase) are present (2theta=34.87°), one can assume that the oxide film thickness is thin enough to expose the metal diffraction pattern.

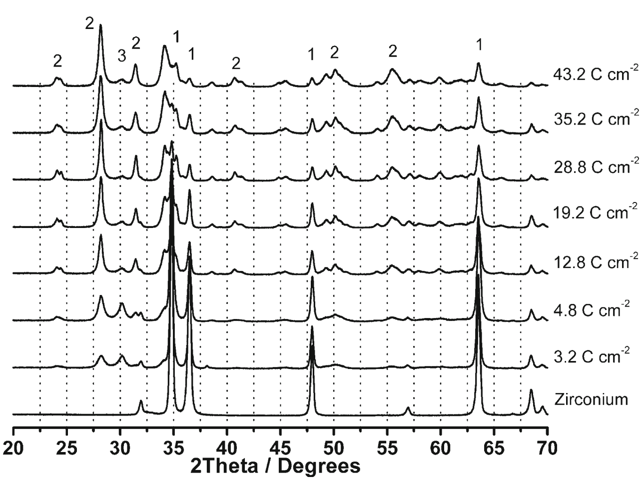

Fig. 4 X-ray diffractograms for films obtained for different anodisation charges. Oxide films were prepared in 0.1 $mol L^{-1}$ phosphoric acid solution, i=16 $mA cm^{-2}$, T=20 °C. *1* Zr hexagonal phase, *2* ZrO_2 monoclinic phase, *3* ZrO_2 tetragonal phase

The microstructure analysis was performed using the GSAS-EXPGUI refinement program and the Le Bail method [58]. It is important to emphasise that the determination of the phase composition using the Rietveld method could not be performed because the anodically prepared zirconium oxide is formed over a zirconium metallic substrate and, in some samples, the phase quantities were not large enough to allow precise quantification. Hence, the Le Bail method was preferred over the Rietveld refinement for analysis of the XRD patterns. This alternative method has some advantages that allow the evaluation of the crystallite size and isotropic strain (internal stress) with high accuracy using the whole XRD spectra. Estimation of phase composition quantities was carried out using a quantitative approach regarding the diffraction peak areas of the most intense *hkl* peaks for a specific phase.

Table 1 depicts the crystallite size and the estimation of phase quantities using the peak area for the monoclinic and tetragonal phases as a function of charge density for ZrO_2. In addition, the estimation of the phase quantities was plotted in Fig. 5 as the ratio of the tetragonal to monoclinic phase during the anodisation. From data presented in Table 1, for all charge densities studied, we observed that the crystallite size for the monoclinic phase exhibits a maximum value just after the Q^T transition region, which is depicted in Fig. 1b (20.3 °$C cm^{-2}$), and then stabilises. We also observed that the isotropic strain variation is constant after 12 °$C cm^{-2}$ (Fig. 6). Hence, the change in peak width in XRD spectra for 28.8 °$C cm^{-2}$ (Table 1) where the maximum crystallite size was observed cannot be associated with the oxide strain variation. At some charge densities, it was not possible to determine the tetragonal crystallite size due to the low concentration of this phase in the oxide film.

Table 1 Crystallite size and peak area for the monoclinic and tetragonal phases as a function of charge density for the ZrO_2 films prepared in 0.1 $mol L^{-1}$ phosphoric acid solution, i=16 $mA cm^{-2}$, T=20 °C

Charge density (C cm−2)	Monoclinic crystallite size (Å)	Tetragonal crystallite size (Å)	Peak area	
			Monoclinic	Tetragonal
3.2	155	63	1,408.9	1,362.3
4.8	361	194	2,206.0	1,825.9
12.8	351	–	2,072.2	493.20
19.2	467	–	2,504.3	392.40
28.8	627	–	2,582.2	437.30
35.2	468	–	2,662.6	436.70
43.2	459	114	3,441.9	437.70

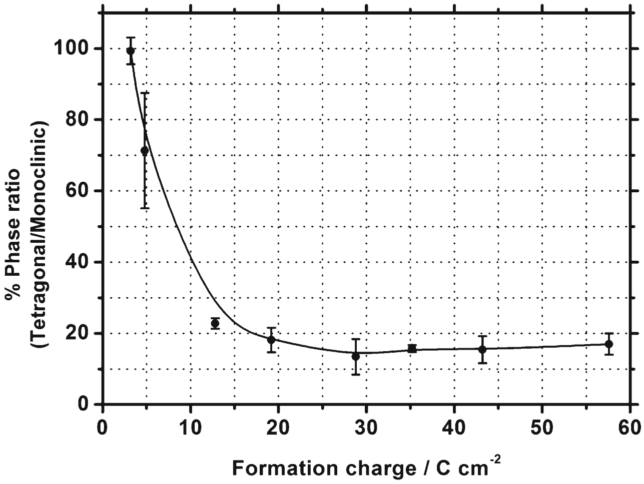

Fig. 5 Tetragonal/monoclinic phase quantity ratio as a function of the formation charge density. Oxide films were prepared in 0.1 molL^{-1} phosphoric acid solution, i=16 mAcm^{-2}, T=20 °C. Phase composition was estimated from the area of the most intense related *hkl* diffraction peak for that phase

According to Fig. 5, after the beginning of the electrolytic breakdown process under PA (3.2 °Ccm^{-2}), a spontaneous transition of phase occurs. It can be observed that the ratio is large at the beginning of the electrolytic rupture and it decreases near the formation charge where Q^{T} was observed. Now, from the perspective of these results, i.e., crystallite size and phase ratios, we can draw an empirical relationship between the Q^{T} and the microstructural variation observed during the electrolytic breakdown. From a qualitatively point of view, it is acceptable that the phase transition and the changes in the monoclinic crystallite size observed in the present work are an indirect consequence of the high local temperature induced from intense discharges (sparks) and the high strain energy from fast oxide growth

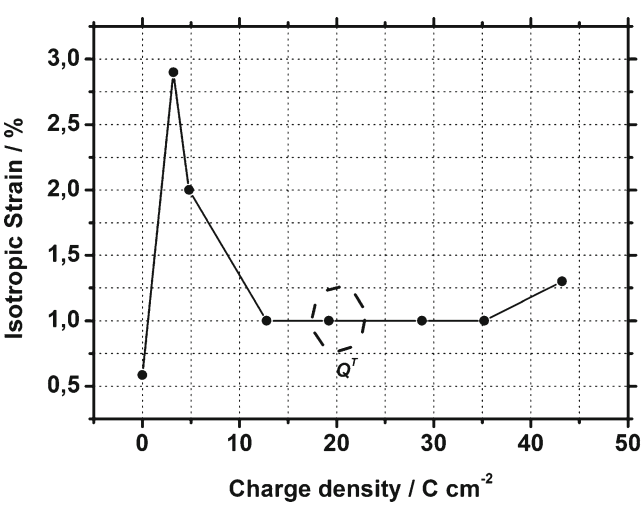

Fig. 6 Isotropic strain of monoclinic phase as a function of charge density. Oxide films were prepared in 0.1 molL^{-1} phosphoric acid solution, i=16 mAcm^{-2}, T=20 °C

observed during the electrolytic breakdown. In the following paragraphs, we will discuss this proposition in detail based on the classical proposed theory for ZrO_2 for solid state oxide phase transition [53, 77, 78].

At the beginning of the breakdown process, the crystallite sizes for both of the detected phases are small, i.e., 15.5 nm and 6.3 nm, for monoclinic and tetragonal phases, respectively. During the electrolytic breakdown initiation, the boundary condition in that stage is such that both monoclinic and tetragonal phases coexist depicting small crystallite size as presented in Table 1. In the literature, deriving from the oxide crystallisation mechanism under high temperatures, the monoclinic crystallite growth can be explained by the consumption of the tetragonal form by means of the continuous phase transition theory [52–54, 77, 78]. According to this theory, whenever a crystal of monoclinic ZrO_2 is heated to a temperature high enough, the domains of the tetragonal phase might form in the monoclinic matrix, and the system is described as a hybrid single crystal in which the two phases coexist. In our case, this transition can occur due to the high strain energy that is associated to the molar volume difference between the two phases. Hence, during ZrO_2 electrolytic breakdown, the strain is high enough to allow perfect phase coexistence, tetragonal and monoclinic, at the beginning of electrolytic breakdown at 3.2 °Ccm^{-2} for PA anodisation (see also Figs. 5 and 6).

Additionally, spark events at this stage of anodisation (before Q^{T}) are very intensive, and several authors have proposed the creation of gas discharge and plasma under conditions where high local temperature at the position of the spark was observed [15–17, 63–65]. Considering that the local spark event is so intense that each event provides enough energy to generate a high concentration of defects, such as oxygen vacancies [78, 79], this could lead to the stabilisation of the tetragonal phase at this anodisation stage [78]. Following the classical propositions related to high temperature phase transition [78], after Q^{T}, it was observed a decrease in the number of spark events distributed over the electrode surface, which indicates a low local temperature at spark sites during the breakdown regime. This condition suggests a monoclinic-preferred formation regime [78]. We also supposed that the amplitude of voltage oscillations observed in the anodisation curve (Fig. 1) can be indicative of how deep and intense the local spark event disrupts the oxide during electrolytic breakdown leading us to assume that after Q^{T}, the "destruction" energy is less intense. However, this "voltage oscillation amplitude" assumption has not yet been demonstrated and more experimental support should be necessary.

Another experimental support for the observed martensitic tetragonal-to-monoclinic transition is derived from a crystal structure twinning between both phases when ZrO_2 phase transformation occurs [53, 54, 80], i.e., the space group of monoclinic ZrO_2 (P21/c) is a subgroup of the tetragonal space group (P42/nmc) [52, 54]. In other words, the tetragonal structure can be derived from the monoclinic structure by suppressing certain symmetry elements of the latter. During this transformation, the monoclinic domains come into contact with the tetragonal domains as the reaction proceeds. If they have different orientations, the twinning can also provide the energy for the phase transition.

In summary, we observed a ZrO_2 phase transition where tetragonal domains are converted to monoclinic ones. This proposition of crystal transformation occurring during the electrolytic breakdown stage is quite reasonable considering the high electrical field and the local energy released during zirconium PEO, where intense spark generation is observed. Therefore, considering the data obtained and literature propositions, the experimental evidence supporting this interpretation is afforded by empirical observations associated with Q^T such as:

1. A change in the voltage oscillation amplitude in the anodisation curve was observed;
2. This change in voltage oscillation amplitude is accompanied by a shift in the numbers of spark events at Q^T which change from a highly intensive regime to a lowly intensive one after Q^T;
3. At Q^T, a steady state in the ratio between tetragonal and monoclinic phase quantity was detected.

Conclusions

A transition in the voltage oscillation amplitude was observed during the electrolytic breakdown for ZrO_2 formation by anodic preparation in oxalic acid or PA solution, called Q^T. This transition is a monotonic function of both temperature and current density, which indicates that Q^T has a physical meaning. X-ray diffraction analysis showed that the ZrO_2 formed is crystalline, and both monoclinic and tetragonal phases were observed at the beginning of the electrolytic breakdown (before Q^T). The presence of both phases before Q^T was explained in terms of the high field strength and the local energy that is released during the PEO over the Zr electrodes, where intense spark generation is observed. This phenomenon could be related to a tetragonal–monoclinic phase transformation that is described by the domain theory, in which the continuous phase transformation occurs via the conversion of the tetragonal phase to the monoclinic stable phase and the stabilisation of the monoclinic phase content after Q^T.

Acknowledgements The authors gratefully acknowledge the financial support from the Brazilian research funding agencies FAPESP and CNPq.

References

1. Vermilyea DA (1955) The crystallization of anodic tantalum oxide films in the presence of a strong electric field. J Electrochem Soc 102(5):207–214
2. Diggle JW, Downie TC, Goulding CW (1969) Anodic oxide films on aluminum. Chem Rev 69(3):365–382
3. Parkhutik VP, Albella JM, Martinez-Duart JM (1992) Eletric breakdown in anodic oxide films. In: Conway B, White J, Bockris JOM (eds) Modern aspects of electrochemistry, vol 23. Plenum, New York, p 391
4. Lohrengel MM (1993) Thin anodic oxide layers on aluminum and other valve metals—high field regime. Mater Sci Eng, R 11 (6):243–294
5. Schultze JW, Lohrengel MM, Ross D (1983) Nucleation and growth of anodic oxide films. Electrochim Acta 28(7):973–984
6. Masuda H, Fukuda K (1995) Ordered metal nanohole arrays made by a 2-step replication of honeycomb structures of anodic alumina. Science 268(5216):1466–1468
7. Masuda H, Yamada H, Satoh M, Asoh H, Nakao M, Tamamura T (1997) Highly ordered nanochannel-array architecture in anodic alumina. Appl Phys Lett 71(19):2770–2772
8. Masuda H, Asoh H, Watanabe M, Nishio K, Nakao M, Tamamura T (2001) Square and triangular nanohole array architectures in anodic alumina. Adv Mater 13(3):189–192
9. Beranek R, Hildebrand H, Schmuki P (2003) Self-organized porous titanium oxide prepared in H2SO4/HF electrolytes. Electrochem Solid-State Lett 6(3):B12–B14
10. Tsuchiya H, Schmuki P (2004) Thick self-organized porous zirconium oxide formed in H_2SO_4/NH_4F electrolytes. Electrochem Commun 6(11):1131–1134
11. Tsuchiya H, Macak JM, Ghicov A, Taveira L, Schmuki P (2005) Self-organized porous TiO_2 and ZrO_2 produced by anodization. Corros Sci 47(12):3324–3335
12. Bensadon EO, Nascente PAP, Olivi P, Bulhoes LOS, Pereira EC (1999) Cubic stabilized zirconium oxide anodic films prepared at room temperature. Chem Mater 11(2):277–280
13. Frauchiger VM, Schlottig F, Gasser B, Textor M (2004) Anodic plasma-chemical treatment of CP titanium surfaces for biomedical applications. Biomaterials 25(4):593–606
14. Trivinho-Strixino F, Guimaraes FEG, Pereira EC (2008) Luminescence in anodic ZrO2 doped with Eu(III)ions. Mol Cryst Liq Cryst 485:766–775
15. Yerokhin AL, Nie X, Leyland A, Matthews A, Dowey SJ (1999) Plasma electrolysis for surface engineering. Surf Coat Technol 122 (2–3):73–93
16. Pauporte T, Finne J, Kahn-Harari A, Lincot D (2005) Growth by plasma electrolysis of zirconium oxide films in the micrometer range. Surf Coat Technol 199(2–3):213–219
17. Yerokhin L, Snizhko LO, Gurevina NL, Leyland A, Pilkington A, Matthews A (2003) Discharge characterization in plasma electrolytic oxidation of aluminium. J Phys D-Appl Phys 36(17):2110–2120
18. Leach JSL, Pearson BR (1984) The conditions for incorporation of electrolyte ions into anodic oxides. Electrochim Acta 29(9):1263–1270
19. Montero I, Albella JM, Martinezduart JM (1985) Influence of electrolyte concentration on the anodization and breakdown characteristics of Ta_2O_5 films. J Electrochem Soc 132(4):814–818
20. Li Y, Shimada H, Sakairi M, Shigyo K, Takahashi H, Seo M (1997) Formation and breakdown of anodic oxide films on aluminum in boric acid borate solutions. J Electrochem Soc 144(3):866–876
21. Dyer CK, Leach JSL (1978) Breakdown and efficiency of anodic oxide—growth on titanium. J Electrochem Soc 125(7):1032–1038
22. Diquarto F, Piazza S, Sunseri C (1984) Breakdown phenomena during the growth of anodic oxide-films on zirconium metal—

influence of experimental parameters on electrical and mechanical breakdown. J Electrochem Soc 131(12):2901–2906
23. Khalil N, Bowen A, Leach JSL (1988) The anodic-oxidation of valve metals.2. The influence of the anodizing conditions on the transport processes during the anodic-oxidation of zirconium. Electrochim Acta 33(12):1721–1727
24. Freitas M, Bulhoes LOS (1997) Breakdown and crystallization processes in niobium oxide films in oxalic acid solution. J Appl Electrochem 27(5):612–615
25. Chiu RL, Chang PH, Tung CH (1995) The effect of anodizing temperature on anodic oxide formed on pure Al thin-films. Thin Solid Films 260(1):47–53
26. Ikonopisov S (1977) Theory of electrical breakdown during formation of barrier anodic films. Electrochim Acta 22(10):1077–1082
27. Albella JM, Montero I, Martinezduart JM (1984) Electron injection and avalanche during the anodic-oxidation of tantalum. J Electrochem Soc 131(5):1101–1104
28. Albella JM, Montero I, Martinezduart JM (1987) A theory of avalanche breakdown during anodic-oxidation. Electrochim Acta 32(2):255–258
29. Diquarto F, Piazza S, Sunseri C (1986) A phenomenological approach to the mechanical breakdown of anodic oxide-films on zirconium. Corros Sci 26(3):213–221
30. Diquarto F, Piazza S, Sunseri C (1988) Electrical and mechanical breakdown of anodic films on tungsten in aqueous-electrolytes. J Electroanal Chem 248(1):99–115
31. Diquarto F, Piazza S, Sunseri C (1988) Electrical breakdown and pitting in anodic films on tungsten in halogen ion-containing solutions. J Electroanal Chem 248(1):117–129
32. Bulygin EV, Sverdlin IA (1994) Pitting during initiation of spark electric breakdown in the process of aluminum anodization in nonaqueous solutions of trialkylammonium alkylcarboxylates. Russ J Electrochem 30(4):513–520
33. Gupta P, Tenhundfeld G, Daigle EO, Schilling PJ (2005) Synthesis and characterization of hard metal coatings by electro-plasma technology. Surf Coat Technol 200(5–6):1587–1594
34. Gupta P, Tenhundfeld G, Daigle EO, Ryabkov D (2007) Electrolytic plasma technology: science and engineering—an overview. Surf Coat Technol 201(21):8746–8760
35. Ikonopisov S, Girginov A, Machkova M (1979) Electrical breaking down of barrier anodic films during their formation. Electrochim Acta 24(4):451–456
36. Diggle JW, Downie TC, Goulding CW (1968) Effect of anodic oxide films on polarization characteristics of Al. Corros Sci 8 (12):907–911
37. Van Overmeere Q, Proost J (2010) Stress-induced breakdown during galvanostatic anodising of zirconium. Electrochim Acta 55(15):4653–4660
38. Proost J, Vanhumbeeck JF, Van Overmeere Q (2009) Instability of anodically formed TiO2 layers (revisited). Electrochim Acta 55 (2):350–357
39. Habazaki H, Shimizu K, Nagata S, Asami K, Takayama K, Oda Y, Skeldon P, Thompson GE (2005) Inter-relationship between structure and dielectric properties of crystalline anodic zirconia. Thin Solid Films 479(1–2):144–151
40. Arora MR, Kelly R (1977) Structure and stoichiometry of anodic films on V, Nb, Ta, Mo and W. J Mater Sci 12(8):1673–1684
41. Vermilyea DA (1957) Nucleation of crystalline Ta_2O_5 during field crystallization. J Electrochem Soc 104(9):542–546
42. Draper PHG, Harvey J (1963) Structure of anodic films.1.An electron diffraction examination of products of anodic oxidation on tantalum, niobium and zirconium. Acta Metall 11(8):873–875
43. Hornkjol S, Hurlen T (1990) Anodic growth of passive films on zirconium and hafnium. Electrochim Acta 35(11–12):1897–1900
44. Michaelis A, Schweinsberg M (1998) An anisotropy microellipsometry (AME) study of anodic film formation on Ti and Zr single grains. Thin Solid Films 313:756–763
45. Neufeld P, Akbar M, Ashdown R, Nagpaul NK (1972) Crystallization of anodic Al_2O_3. Electrochim Acta 17(9):1543
46. Leach JSL, Pearson BR (1988) Crystallization in anodic oxide-films. Corros Sci 28(1):43–56
47. Adams GB, Vanrysselberghe P (1955) Anodic polarization of zirconium at low potentials—formation rates, formation field, electrolytic parameters, and film thicknesses of very thin oxide films. J Electrochem Soc 102(9):502–511
48. Archibald LC, Leach JSL (1977) Anodic-oxidation of zirconium.1. Growth stresses in anodic ZrO2 films. Electrochim Acta 22(1):15–20
49. Archibald LC, Leach JSL (1977) Anodic-oxidation of zirconium.2. Growth and morphology of anodic ZrO2 films. Electrochim Acta 22(1):21–25
50. Vanhumbeeck JF, Proost J (2008) On the contribution of electrostriction to charge-induced stresses in anodic oxide films. Electrochim Acta 53(21):6165–6172
51. Vanhumbeeck JF, Proost J (2008) On the relation between growth instabilities and internal stress evolution during galvanostatic Ti thin film anodization. J Electrochem Soc 155(10):C506–C514
52. Grain CF, Garvie RC (1965) Mechanism of monoclinic—tetragonal transformation of zirconium dioxide. Am Ceram Soc Bull 44 (4):315–320
53. Garvie RC (1965) Occurrence of metastable tetragonal zirconia as a crystallite size effect. J Phys Chem 69(4):1238–1243
54. Alper AM (1970) High temperature oxides. Part II: oxides of rare earths, titanium, zirconium, hafnium, niobium and tantalum. In: Margrave JL (ed) Refractory materials: a series of monographs, vol 5-II. vol 5/6. Academic, New York, p 276
55. Salas P, De la Rosa-Cruz E, Diaz-Torres LA, Castano VM, Melendrez R, Barboza-Flores M (2003) Monoclinic ZrO_2 as a broad spectral response thermoluminescence UV dosemeter. Radiat Meas 37 (2):187–190
56. Ciosek J, Paszkowicz W, Pankowski P, Firak J, Stanislawek U, Patron Z (2003) Modification of zirconium oxide film microstructure during post-deposition annealing. Vacuum 72(2):135–141
57. Lin CK, Zhang CM, Lin J (2007) Phase transformation and photoluminescence properties of nanocrystalline ZrO_2 powders prepared via the Pechini-type sol–gel process. J Phys Chem C 111(8):3300–3307
58. Bail AL, Duroy H, Fourquet JL (1988) Ab-initio structure determination of $LiSbWO_6$ by X-ray powder diffraction. Mater Res Bull 23(3):447–452
59. Larson AC, Dreele RBV (2000) GSAS (general structure analysis system). Used version: August 1997 edn., Los Alamos National Laboratory Report LAUR 86-748
60. Toby BH (2001) EXPGUI, a graphical user interface for GSAS. J Appl Crystallogr 34:210–213
61. Morrison SR (1980) Electrochemistry at semiconductor and oxidized metals electrodes. Plenum, New York
62. Dewit HJ, Wijenberg C, Crevecoeur C (1976) Dielectric-breakdown of anodic aluminum-oxide. J Electrochem Soc 123 (10):1479–1486
63. Matykina E, Doucet G, Monfort E, Berkani A, Skeldon P, Thompson GE (2006) Destruction of coating material during spark anodizing of titanium. Electrochim Acta 51(22):4709–4715
64. Matykina E, Berkani A, Skeldon P, Thompson GE (2007) Real-time imaging of coating growth during plasma electrolytic oxidation of titanium. Electrochim Acta 53(4):1987–1994
65. Hussein RO, Nie X, Northwood DO, Yerokhin A, Matthews A (2010) Spectroscopic study of electrolytic plasma and discharging behaviour during the plasma electrolytic oxidation (PEO) process. J Phys D-Appl Phys 43(10):1–13

66. Leach JSL, Pearson BR (1984) The effect of foreign ions upon the electrical characteristics of anodic ZrO_2 films. Electrochim Acta 29 (9):1271–1282
67. Bradhurs DH, Leach JSL (1966) Mechanical properties of thin anodic films on aluminum. J Electrochem Soc 113(12):1245–1255
68. Davies JA, Domeij B, Pringle JPS, Brown F (1965) The migration of metal and oxygen during anodic film formation. J Electrochem Soc 112:675–680
69. Pringle JPS (1980) The anodic-oxidation of superimposed metallic layers—theory. Electrochim Acta 25(11):1423–1437
70. Parkhutik VP, Makushok YE, Kudryavtsev VI, Sokol VA, Khodan AN (1987) X-ray photoelectron study of the formation of anodic oxide-films on aluminum in nitric-acid. Soviet Electrochemistry 23 (11):1439–1444
71. Parkhutik V, Gomez FC, Tarazona LM, Esteve RF (2000) Oscillatory kinetics of anodic oxidation of silicon—influence of the crystallographic orientation. Microelectron Reliab 40(4–5):795–798
72. Parkhutik V, Matveeva E, Perez R, Alamo J, Beltran D (2000) Mechanism of large oscillations of anodic potential during anodization of silicon in H3PO4/HF solutions. Mater Sci Eng B-Solid State Mater Adv Technol 69:553–558
73. Parkhutik V (2001) Silicon anodic oxides grown in the oscillatory anodisation regime—kinetics of growth, composition and electrical properties. Solid-State Electron 45(8):1451–1463
74. Parkhutik V (2002) Chaos-order transitions at corroding silicon surface. Mater Sci Eng B-Solid State Mater Adv Technol 88(2–3):269–276
75. Parkhutik VP (2006) Oscillations of open-circuit potential during immersion plating of silicon in CuSO4/HF solutions. Russ J Electrochem 42(5):512–522
76. Shimizu K, Kobayashi K, Skeldon P, Thompson GE, Wood GC (1997) Anodic oxidation of zirconium covered with a thin layer of aluminium. Thin Solid Films 295(1–2):156–161
77. Garvie RC (1978) Stabilization of tetragonal structure in zirconia microcrystals. J Phys Chem 82(2):218–224
78. Shukla S, Seal S (2005) Mechanisms of room temperature metastable tetragonal phase stabilisation in zirconia. Int Mater Rev 50(1):45–64
79. Trivinho-Strixino F, Guimaraes FEG, Pereira EC (2008) Zirconium oxide anodic films: optical and structural properties. Chem Phys Lett 461(1–3):82–86
80. Garvie RC, Goss MF (1986) Intrinsic size dependence of the phase-transformation temperature in zirconia microcrystals. J Mater Sci 21(4):1253–1257